

Quantum Arithmetic-based on Quantum Signal Processing

Robin OLLIVE and Stephane LOUISE

Université Paris-Saclay, CEA, List, F-91120, Palaiseau, France

As in classical reversible computing, Quantum Arithmetic is typically seen as a set of tools that process binary data encoded into a quantum register to set the value of another quantum register. This article presents another approach to explain the Quantum Arithmetic in quantum computing. Here, Quantum Arithmetic is addressed with a matrix processing point of view. Quantum Arithmetic is a convenient way to construct the Query that implements the mathematical problem of interest. This approach is not only an interpretation with the matrix approach to encode the problem of interest; it also allows us to derive a new original technique to construct Quantum Arithmetic with the framework of embedded Quantum Signal Processing (QSP). This work uses the link between the eigenstate amplitude and the operator phase to transform the QSP processed amplitude into binary value extracted by Quantum Phase Estimation (QPE). The explanations allowing the QSP based Quantum Arithmetic construction let appear natively sub-routines and functions used by well-known algorithms such as Ancilla Quantum Encoding (AQE)'s Harrow–Hassidim–Lloyd algorithm (HHL) and Quantum Amplitude Estimation (QAE). Methods to implement this circuit are presented in the paper.

Contents

1	Introduction	3
2	Quantum Arithmetic based query	3
2.1	Hamiltonian Simulation-based Quantum Arithmetic	5
2.2	Quantum Arithmetic-based Block-Encoding and projector as specific HHL .	6
3	Quantum Signal Processing-based Quantum Arithmetic	7
3.1	QFT-based adder	7
3.1.1	Quantum Phase Estimation Interpretation of the Quantum Fourier Transform Adder	8
3.2	Quantum Signal Processing-based Quantum Arithmetic	8
3.2.1	Illustrative Example	10
3.2.2	Binary number to Quantum Amplitudes	10
3.2.3	Amplitude Proceeding	11
3.2.4	Oracle Construction: Amplitudes Flagging	12
3.2.5	Amplitudes to Binary Register	13
3.2.6	Scaling and Comparison	16
3.2.7	Quantum Signal Estimation with Arbitrary Parity	17
4	Conclusion	17
5	Funding	20
A	Appendix: Phase Angle Series	20
B	Annex: Link with other Quantum Routines	22
B.1	Ancilla Quantum Encoding: large angle correction	22
B.2	Link with Quantum Amplitude Estimation	22
C	Annex Phase Kick-back: Quantum Arithmetic based Hamiltonian Simulation	24
D	Annex: Embedded Quantum Signal Processing and Quantum Phase Estimation	25
D.1	Essential details about Quantum Signal Processing Semantic Embedding . .	25
D.2	Important details about Quantum Phase Estimation of a Quantum Signal Processing Semantic Embedding Result	28

1 Introduction

Many quantum algorithms need Quantum Arithmetic as a subroutine. Shor’s algorithm [1], certain Grover Oracles [2], and one of the HHL [3] sub-routines rely on Quantum Arithmetic [4, Table.11]. The ability to compute functions of binary numbers is required to implement or process many classical problems in a quantum computer. Many quantum algorithms process a superposition of binary numbers, which allows the associated problem to be solved efficiently.

Quantum Arithmetic is often constructed with two strategies. These strategies are based on either the binary logic bitwise adders [5] assembly [6, 7] or the Quantum Fourier Transform (QFT) phase adders [8] assembly [9–12]¹. Both these strategies combine these simple blocks to elaborate complex functions. It can lead to polynomial approximations of arbitrary functions [15]. Many developments to improve, categorize and evaluate them exist in the literature [4, 16]. This part of the algorithm has an extensive cost of quantum resources due to the high number of required ancilla qubits. These ancilla qubits are needed to store the intermediate results [15]. The trade-off between the number of ancilla qubits and the number of operations is one of the key aspects in designing a quantum circuit for Quantum Arithmetic.

Recent developments in quantum algorithms allow to interpret the implemented problem as qubitized matrices and bring a routine, the QSP [17–21], that competes with HHL to process the matrices. The QSP and its generalization, the Quantum Singular Value Transformation (QSVT) [22] routine allow the processing of real part of matrix amplitudes. QSP does polynomial functions of the amplitudes with the polynomial order equal to the number of matrix repetitions [21]. Composing layers of QSP and therefore function composition is possible using the more restrictive embedded QSP or QSVT [23]. It gives access to more complex functions. Using these tools in order to construct Quantum Arithmetic with a smooth function process thanks to Quantum Signal Processing is the core idea of this paper. The idea of avoiding Quantum Arithmetic to construct a function was already developed in [24] to prepare a quantum state.

This article proposes two contributions. The first contribution is to show the links between Quantum Arithmetic and the other techniques of problem implementation. It explains the QFT-based adder structure directly. This part shows why it implies that projector constructs from Quantum Arithmetic are a particular HHL instance. The second contribution is an original strategy to construct the Quantum Arithmetic routines. This strategy is not based on a combination of simple operations. Instead, thanks to well-tuned QSP techniques, the function of the binary register is computed in the amplitudes of the ancilla qubit. Depending on the reason why the Quantum Arithmetic is constructed, this amplitude can be read into a third register thanks to a QPE variant, or directly transformed into a Grover oracle, or state initialization. We give an example with the complete set of parameters that allow the implementation. Depending on the function of the binary register, this method can be more efficient, especially regarding the number of ancilla qubits.

2 Quantum Arithmetic based query

To solve problems with quantum algorithms, the first thing that must be checked is whether or not the classical problem can be formulated with quantum information. If so, then this

¹A recent approach proposes to construct a more efficient QFT-based multiplier directly [13]; nevertheless, a deep analysis of the sub-routines seems to cancel this advantage [14].

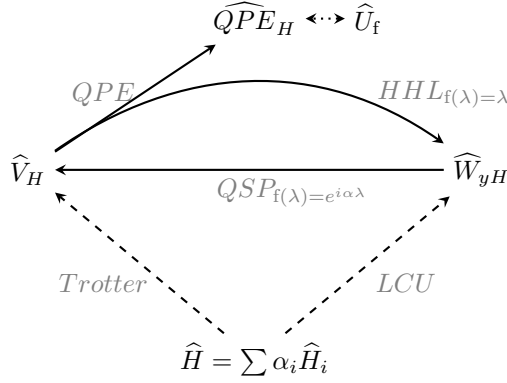


Figure 1: Conversion between the different Query used to process information into QPU. The dotted and dashed lines represent the classical data implementation, while the filled lines represent data processing on the QPU.

quantum information must be implemented as a quantum unitary gate, the query, which can be processed by the Quantum Processing Unit (QPU). Two very popular queries are Hamiltonian Simulation eq. (1) and Block-Encoding² eq. (2). A third one, that encodes the same quantum information is the results from a QPE algorithm eq. (3). It is often more complicated to construct it. The QPE result is often used to read the information because it contains the binary representation of the matrix eigen-phases λ_i with the associated eigenstate $|\lambda_i\rangle$, which can easily be read.

$$\widehat{V}_H = e^{i2\pi \frac{1}{\lambda_{max}} \widehat{H}} \quad (1)$$

$$\widehat{W}_{yH} = \begin{bmatrix} \widehat{H} & -\sqrt{\widehat{I} - \widehat{H}^2} \\ \sqrt{\widehat{I} - \widehat{H}^2} & \widehat{H} \end{bmatrix} \begin{bmatrix} |\psi\rangle |\psi_{\parallel}\rangle \\ |\psi\rangle |\psi_{\perp}\rangle \end{bmatrix} \quad (2)$$

with $|\psi_{\parallel}\rangle$ and $|\psi_{\perp}\rangle$ some control states.

$$\widehat{QPE}_H = \sum_i |\lambda_i\rangle \langle \lambda_i| \otimes |\text{bin}[(b + \lambda_i) \bmod [2^F]]\rangle \langle \text{bin}[b]| \quad (3)$$

Since all these queries contain the same information, switching from query to query with another query assembly Fig. 1 is possible.

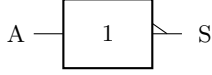
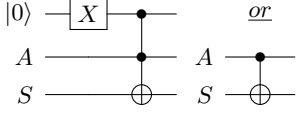

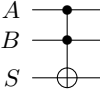
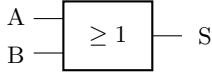
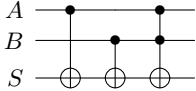
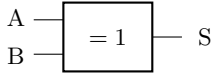
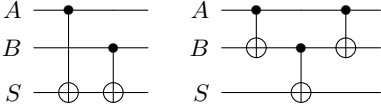
Another way to load the problem's data into the QPU, the Quantum Arithmetic (4), can be used for binary information:

$$\begin{aligned} \widehat{U}_f &= \sum_{x=0}^{2^F} |\text{bin}[x]\rangle \langle \text{bin}[x]| \otimes |\text{bin}[(b + f(x)) \bmod [2^F]]\rangle \langle \text{bin}[b]| \\ \widehat{U}_f |\text{bin}[x]\rangle |0\rangle &= |\text{bin}[x]\rangle |\text{bin}[f(x) \bmod [2^F]]\rangle \end{aligned} \quad (4)$$

While Hamiltonian Simulation and Block-Encoding are based on a decomposition of the matrix formulation of the problem on a family of matrices accessible by the quantum

²Different types of Block-Encoding exist. As soon as the matrix of interest is probabilistically applied to the vector of interest with a control register, the gate is a Block-Encoding. The example of this paper is a specific case called signal operator in the Y-convention due to his behavior when called in a QSP algorithm.

Table 1: Classical logic gates with a quantum computer.
The S qubit begin in the $|0\rangle$ state.

Name:	Classical circuit:	Quantum circuit:
Not / nifter		
AND / \times		
OR / +		
XOR		

algorithm (Fig. 1, dashed lines), Quantum Arithmetic is based on the assembly of basic logical operations. Using the Toffoli gate and X gate, the universal gate of reversible classical logic, all the logical operations can be implemented similarly to the classical logic circuit Table 1 [6, Section 3].

The goal of this section is to show that Quantum Arithmetic has the same shape as a QPE result (Fig. 1, dotted lines). It will also be shown later that the two other aforementioned queries can be constructed from this QPE result to encode a mathematical function.

2.1 Hamiltonian Simulation-based Quantum Arithmetic

Let us start with an operator \hat{H}_f whose application on a binary state associates to this state an amplitude equal to the function image of the binary value:

$$\begin{aligned}\hat{H}_f |\text{bin}[x]\rangle &= f(x) |\text{bin}[x]\rangle \\ \Rightarrow \hat{H}_f &= \sum_{x=0}^{2^F} f(x) |\text{bin}[x]\rangle \langle \text{bin}[x]| \end{aligned} \quad (5)$$

In order to transform this operator into a quantum gate, the normalized³ Hamiltonian Simulation of this operator is implemented:

$$\begin{aligned}\hat{V}_f &= e^{i2\pi \frac{1}{\max[f]} \hat{H}_f} \\ \Rightarrow \hat{V}_f &= \prod_{x=0}^{2^F} e^{i2\pi \frac{f(x)}{\max[f]} |\text{bin}[x]\rangle \langle \text{bin}[x]|} \end{aligned} \quad (6)$$

This gate contains the same quantum information as the Quantum Arithmetic associated with this function (for a function exactly computable *i.e.* with enough qubits on the

³The normalization guarantees a bijective function over the interval.

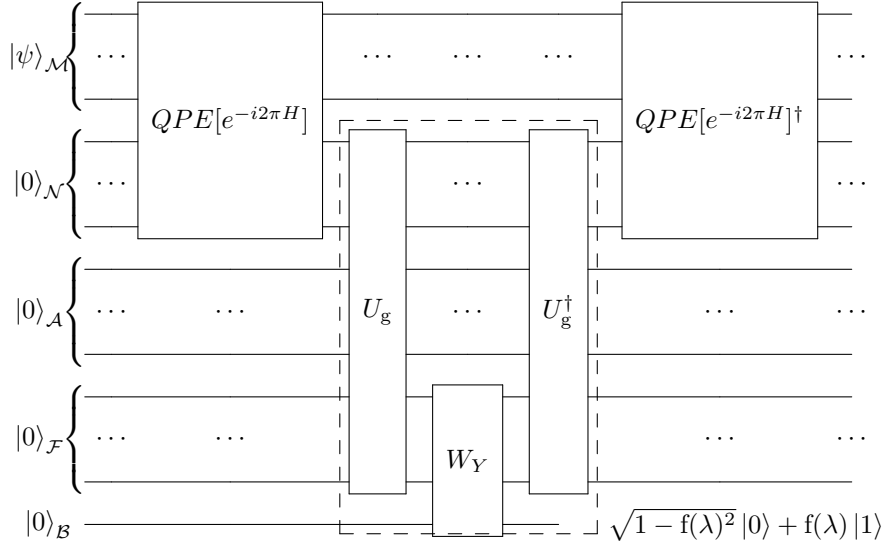


Figure 2: HHL quantum circuit, the dashed box: the AQE, can be understood as making the same function on a matrix diagonal in the computational basis. W_Y is used as a short notation for $C^F\{|\text{bin}[x]\rangle\}R_Y(x)$ which can be constructed as Fig. 3.

output register). It is interesting to note that as for encoding an optimization problem, this gate is a diagonal matrix on the computational basis. The Quantum Arithmetic can be recover thanks to a QPE:

$$\begin{aligned} \widehat{QPE}_{V_f} |\text{bin}[x]\rangle |0\rangle &= |\text{bin}[x]\rangle |\text{bin}[f(x)]\rangle \\ \widehat{QPE}_{V_f} &\Leftrightarrow \widehat{U}_f \end{aligned} \quad (7)$$

Provided that the function Hamiltonian Simulation is accessible, it thus gives an original strategy to produce the Quantum Arithmetic routine. It is already used to construct QFT-based adders but currently not for more complex functions. The generalization is developed during the second part of the paper.

2.2 Quantum Arithmetic-based Block-Encoding and projector as specific HHL

An important utilization of the Quantum Arithmetic is to process quantum information (eigenstate amplitudes) with a function (classical information) thanks to the HHL algorithm Fig. 2. This kind of queries implements properties of the function by selectively altering some states to apply a function on the amplitude of the states of interest. To do so, the Quantum Arithmetic is called in a sub-routine called AQE as illustrated in the dashed box of Fig. 2. The Quantum Arithmetic computes the function composition of $g = \text{p2a} \circ f$, with f the target matrix function and p2a a specific arcsin function [15], detailed in Section 3.2.2, that correct the $\sin(x) - x$ error of the Block-Encoding. In [24], a similar function composition is used to associate the amplitudes function depending on binary inputs.

If the interpretation of the previous section is injected in the HHL algorithm, it directly leads to Quantum Arithmetic-based query. As the Quantum Arithmetic can be understood as the QPE result of a diagonal matrix, the HHL without QPE can be understood as the matrix function of a matrix which is diagonal in the computational basis.

A very popular Quantum Arithmetic-based query is the projector Fig. 4. The projector

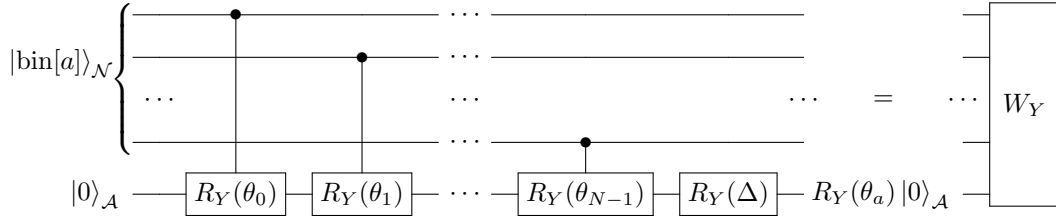


Figure 3: Y -rotationnal-gate kickback also referred as the $C^F\{|\text{bin}[x]\rangle\}R_Y(x)$ gate. This circuit is a \widehat{W}_Y signal operator. In this diagram, $\theta_i = 2\pi \frac{2^i}{\alpha 2^N}$ and $\Delta = 2\pi \frac{\delta}{\alpha}$ and $\theta_a = 2\pi \frac{a}{\alpha 2^N}$.

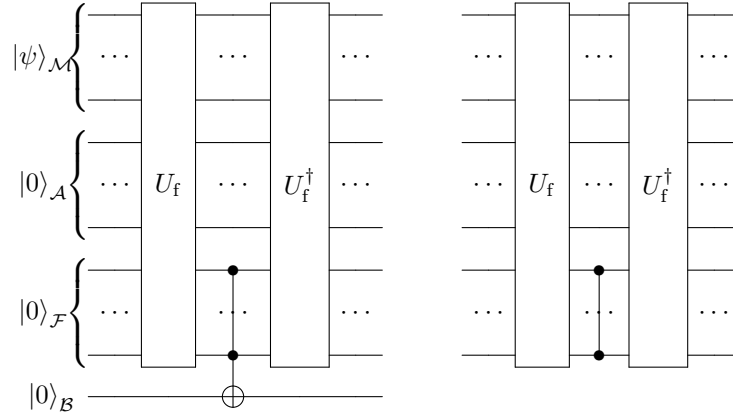


Figure 4: Projector (1) and Grover oracle (2). The n -controlled gate identifies the state $|\text{bin}[y]\rangle$ so that the qubit of the register \mathcal{B} is in $|1\rangle$ for the component of ψ so that $f(\text{bin}[\psi]) = y$. Instead of switching the \mathcal{B} qubit, the oracle switches the sign of the corresponding state.

corresponds to an HHL whose associated function is a specific gate function located on the states selected thanks to Quantum Arithmetic. This Well-functions AQE can be reduced to a multi-controlled gates. This multi-controlled gate applied on the function images register allows to select the state of interest. A Grover's oracle Fig. 4, which marks the state identified by the projector, can easily be constructed by switching the multicontrolled-NOT gates by multicontrolled-phase gates.

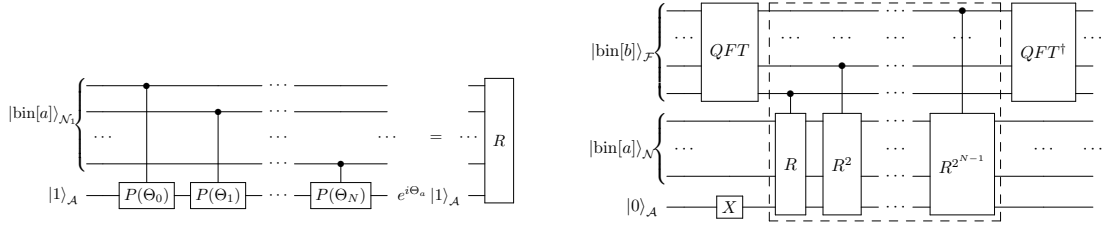
Another query of interest: the Block-Encoding of the \widehat{H}_f : \widehat{W}_{yH_f} is construct if the HHL function is the identity function: $f(x) = x$. It is a general property, HHL, with the identity function constructs the Block-Encoding associated hermitian matrix Block-Encoding.

3 Quantum Signal Processing-based Quantum Arithmetic

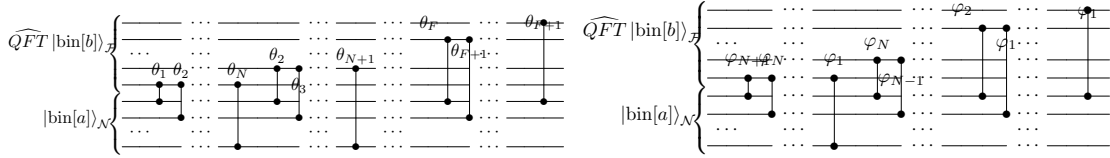
This section describes how to implement Quantum Arithmetic from the QSP phase angles instead of many logical operations.

3.1 QFT-based adder

The first step to achieve Quantum Signal Processing-based Quantum Arithmetic, is the QFT-based adder, which is already used to sum values due to phase additivity. It is the opposite of the phase kickback technique in which binary logic is used to construct a phase: it uses phases to construct binary logic, [25,26] . In the literature, QFT-based adders are



(a) Phase Rotation matrix quantum circuit. The control phase gate is symmetric, so the control side can be switched. In this diagram, $\Theta_i = \pi \frac{\alpha 2^i}{2^F}$ and $\Theta_a = \pi \frac{\alpha a}{2^F}$. (b) Phase reading quantum circuit. The dashed box contains the phase kickback of the phase matrix. At the end of the quantum circuit, the \mathcal{F} register ends in the $|\text{bin}[a+b]\rangle$ state.



(a) Reordered cleaned phase kickback quantum circuit. Note that (since θ is modulo 2π): $\theta_{F+m} = \theta_{F+1-j}$. Here, we choose $F = N + 1$, which is enough for a simple addition. All the lines for which \mathcal{F} label > \mathcal{N} label goes from θ_N to θ_F ($F - N$ terms).

used as a basic logic operation to construct more complex functions. It explains the phase additivity properties; one or many values can be added to a binary register.

3.1.1 Quantum Phase Estimation Interpretation of the Quantum Fourier Transform Adder

The QFT-based quantum adder was introduced as a well-adjusted frequency reading [8, 9, Section 4] or with quantum dictionary [27]. This section aims to evince it as a matrix phase reading thanks to the QPE algorithm. The matrix of interest is diagonal with the 2^N phases associated with the corresponding binary values. Thanks to the controlled-phase-adding, only the values stored in the binary register has a non-zero amplitude and are thus added, Cf. Fig. 5a. Then, the phase reported on this qubit can be read thanks to the QPE algorithm, Fig. 5b. The qubit on which the phase is reported being an ancilla, it can be withdrawn. Therefore, the two interpretations lead to the same quantum circuit Fig. 6a & Fig. 6b.

3.2 Quantum Signal Processing-based Quantum Arithmetic

The QPE interpretation of the QFT adder tells us that other matrices carrying the phase of interest can be chosen. Processing the phase before reading it can be advantageous to construct Quantum Arithmetic. The following subsection combines existing tools allowing the processing of the phase of specific matrices, Fig. 7. Three main steps are needed to construct the routine (called QSE), which are presented in a top-down approach:

1. Assign an entangled phase proportional to the binary representation of each register.
2. Process the phase value with the function of interest.
3. Either read the phase, amplify or mark the result of interest to produce a useful quantum subroutine.

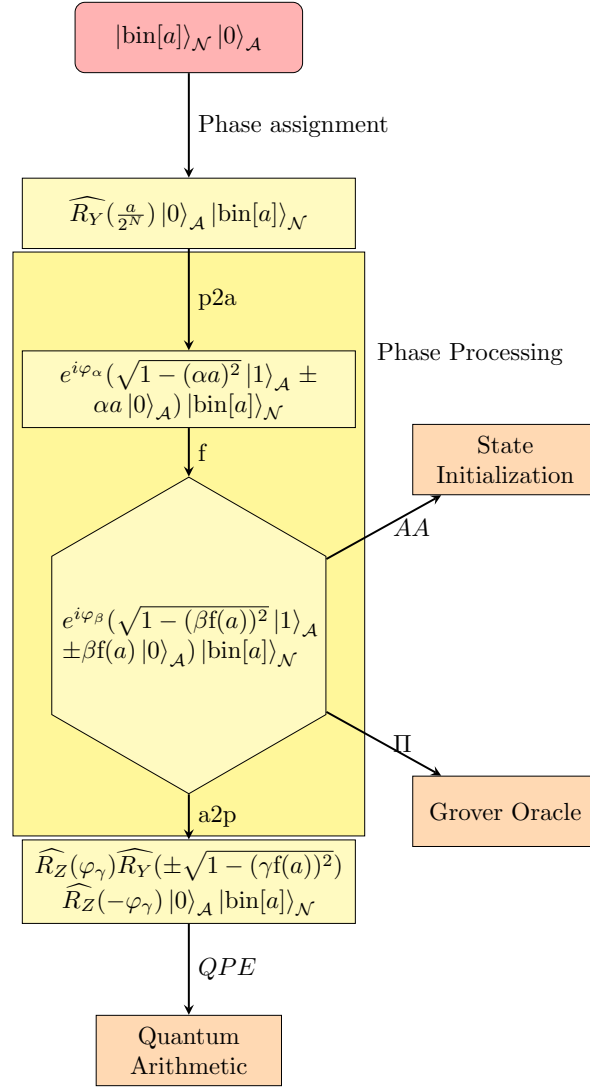


Figure 7: Workflow: Quantum Arithmetic from embedded QSP and QPE. α , β and γ are normalization factors. Π referred to as a gate function and AA refer to as Amplitude Amplification.

The more challenging part is to apply a function to the phases. Three strategies based on QSP variants can be used to construct the function image:

- The QSP semantic embedding which allows to do function composition.
- The usual QSP directly with the function composition: $\text{a2p} \circ f \circ \text{p2a}$ whose phase angles may be hard to find coupled with a QAE to measure the resulting amplitudes.
- Process directly the quantum phases with an usual QSP (simplified Quantum Phase Processing (QPP)) [28].

The QSP semantic embedding strategy is detailed in this article. It can be developed in four stages according to Fig. 7:

1. Block-Encoding amplitudes corresponding to a rotation with a phase proportional to the register's value.

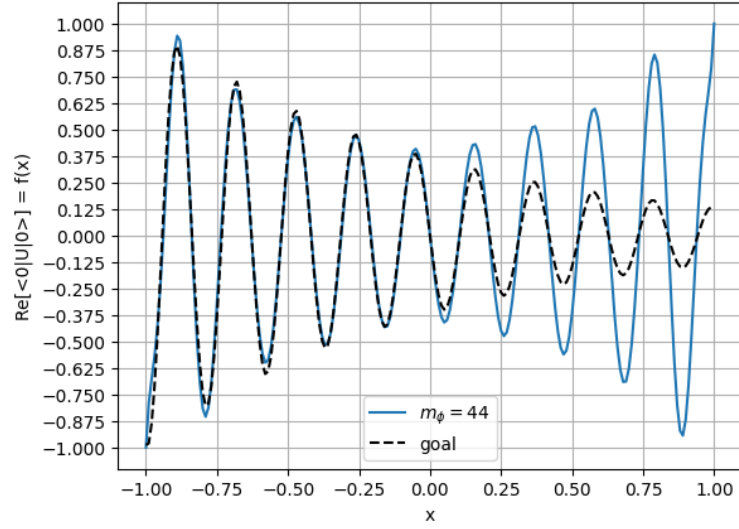


Figure 8: Full representation of the function that will be processed thanks to QSE algorithm variants.

2. Transform the Block-Encoding amplitudes in values proportional to the register's value thanks to embedded QSP.
3. Transform this amplitude in their function images thanks to embedded QSP. This routine is very useful for constructing state preparation, as proposed by [24].
4. Converting these amplitudes into phases proportional to these amplitudes of the Bloch-sphere thanks to embedded QSP.

3.2.1 Illustrative Example

The following sections illustrate the process Fig. 7 with the following function Fig. 8:

$$f(x) = -\cos(15x)e^{-x}$$

To implement it, the following function:

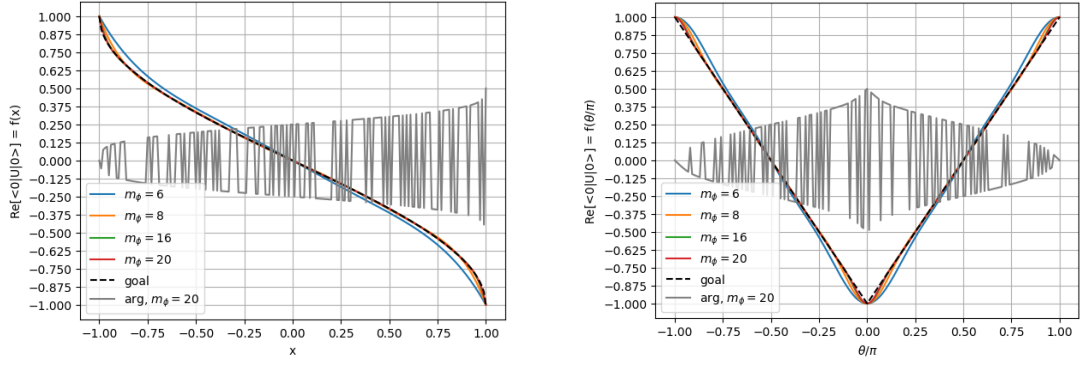
$$\sin(30x)e^{-(1+x)}$$

is prepared on a larger space. Using a larger space allows to eliminate parity constraints of the embedded QSP at the cost of a higher polynomial approximation order. This example of the Quantum Signal Estimation technique encodes this function in the matrix, amplitudes, then phases, to construct a Quantum Arithmetic routine or a Grover oracle.

3.2.2 Binary number to Quantum Amplitudes

To be able to process the quantum phases thanks to embedded QSP, the first objective is to construct an operator that associates to each register's binary representation an amplitude whose real part is proportional to the register's value.

This ability is also needed in the HHL algorithm and is often called AQE. The simplest way to achieve it is to stay in the small angle region where the approximation $x \simeq \sin(x)$ is acceptable and perform a kickback with a Y -rotational-gate Fig. 3.



(a) Approximation of the p2a function with respect to the state amplitude function at different degree m_ϕ . (b) Approximation of the p2a function with respect to the state eigen-phase function at different degree m_ϕ . The amplitude image of a phase with respect to this function will be proportional to the input phase.

Table 2: Some useful subspaces to begin the phase processing thanks to embedded QSP

x	Subspace	shift: δ	scaling coef: α
	$[-1; 1]$	0	1
	$[-1; 0]$	0	2
	$[0; 1]$	1	2
	$[-\frac{1}{2}; \frac{1}{2}]$	$\frac{1}{2}$	2
	$[\frac{1}{4}; \frac{3}{4}]$	$\frac{5}{2}$	4

This matrix Block-Encoding has the shape of a y-rotational-gate so that it can be used as a \widehat{W}_Y embedded QSP signal operator gate. In order to exploit all the amplitude spectrum, a first QSP with the p2a function (8) linearize the cosine (9) in the interval of interest. Its associated phase angles are in Table 4.

$$\begin{aligned} \text{p2a}(x) &= \frac{2}{\pi} \cos^{-1}(x) - 1 \\ &= -\frac{2}{\pi} \sin^{-1}(x) \end{aligned} \quad (8)$$

$$\text{p2a}(\cos(\theta_a + \Delta)) = \frac{a}{\alpha 2^N} + \frac{\delta}{\alpha} - 1 \quad (9)$$

The choice of the subspace in which the amplitudes are projected on depends on our function of interest and is controlled by two parameters, Table 2. When processing the quantum phase, it is essential to keep in mind that the QSP semantic embedding have imposed value for $x \in [-1, 0, 1]$ and that working in a smaller space can leverage it. It is a reason why working on subdomains of x is interesting. The other reason is parity constraints, which is addressed in Section 3.2.7.

3.2.3 Amplitude Proceeding

This part directly depends on the Quantum Arithmetic function of interest. Here, the function f is used as an example, Fig. 10. The unitarity of the matrix processed by QSP imposes that the function must be normalized and evaluated on an interval between $[-1, 1]$:

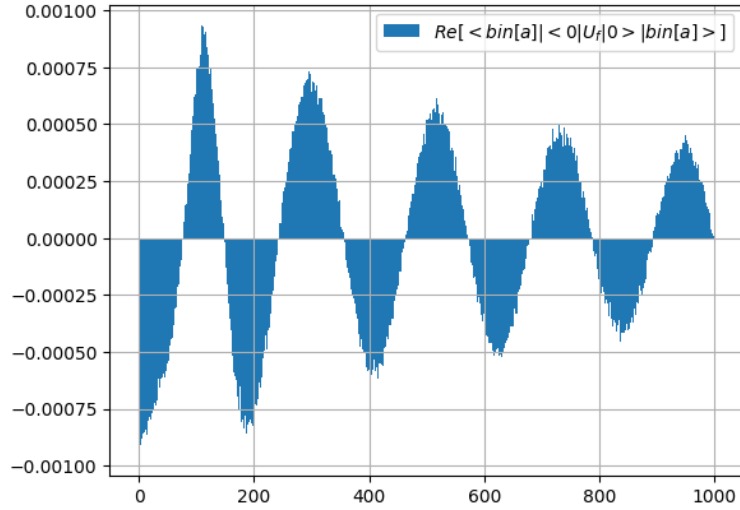


Figure 10: The real part of the quantum amplitudes resulting from the QSP with the phase angles resulting from the merging of p2a and f: Fig. 11 without sgn function. This histogram amplitudes are obtained thanks to a Hadamard test. The QSP is run on a uniform superposition of the register \mathcal{N} . The resulting amplitudes of the real part are thus proportional to the QSP function image of \mathcal{N} register associated value. Here: $N = 10$, $\delta = 0$ and $\alpha = 2$. The number of states is the number of possible binary representations $\max[\text{bin}[a]] = 2^N = 1024$ and $\max[\text{Re}[\langle \text{bin}[a] | \langle 0 | \hat{U} | 0 \rangle | \text{bin}[a] \rangle]] = \frac{1}{2^N} \simeq 0.00097$.

$$f : \{-1; 1\} \longrightarrow \{-1; 1\} \quad (10)$$

The example's set of phase angles can be found in Table 4.

This method does not allow direct quantum state initialization because the amplitudes are block-encoded. As in [24], the amplitude can be amplified with Exact Amplitude Amplification (EAA) to construct a state-initialization.

3.2.4 Oracle Construction: Amplitudes Flagging

This section combines the tools to construct a Grover oracle that flags all the state-respecting constraints. This is done in two steps:

- Construct a quantum state that contains the function of interest thanks to p2a and the phase angles associated with the function of interest. The corresponding quantum circuit is illustrated in Fig. 11.
- Use a filtering function that projects the value of interest to -1 and the other to 1 . For instance:
 - Sign-function (11) allows to seek all the function's positive (or negative) values Fig. 12a. The phase angles of different degrees can be found in Table 4.
 - Step-function (12) allows to seek the roots of the function values of the function Fig. 12b. The phase angles of different degrees can be found in Table 4.

$$\text{sgn}(x) = \frac{x}{|x|} \quad (11)$$

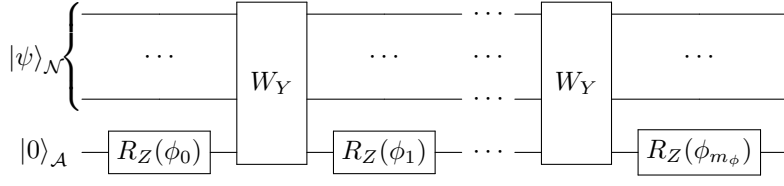
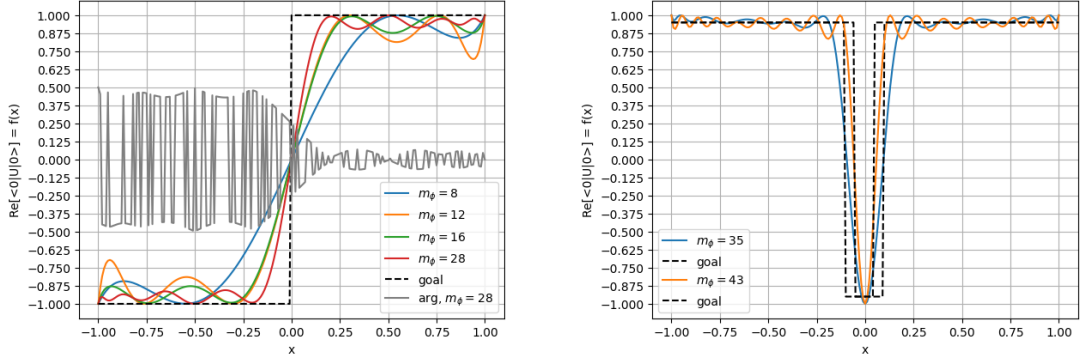


Figure 11: The developed Quantum Signal Oracleization or \widehat{W}_{YH_f} quantum circuit. It uses Fig. 3 with ϕ the phase angle merging following (36) p2a, funct and sgn for the oracle and only p2a and funct for \widehat{W}_{YH_f} .



(a) Approximation of the sgn function with respect to the state amplitude function at different degrees m_ϕ . (b) Approximation of the $\text{step}_{1/20}$ (orange) and $\text{step}_{1/10}$ (blue) function with respect to the state amplitude function.

$$\text{step}_{\delta_s}(x) = -1 \text{ if } |x| < \delta_s; 1 \text{ else} \quad (12)$$

The scaling of this technique is detailed in Table 3 under the name of Quantum Signal Oracleization (QSO).

3.2.5 Amplitudes to Binary Register

In a fashion similar to how QAE is used, reading the phase of a \hat{R}_X or \hat{R}_Y gate results in measuring an arcsine function of its amplitude [29, Section 4: p.18]. Since the goal is not to read the arcsine but the amplitude value, an important step is to convert the amplitude in a phase which is proportional to this amplitude before reading the previous QSP. This is done with the amplitude to phase function (a well-parametrized sine) (13)⁴, Fig. 14a and Fig. 14b.

It results in reading the polynomial approximation of the function in a specific binary format.

$$\text{a2p}(x) = \sin\left(\frac{\pi}{2}x\right) \quad (13)$$

$$\pm \frac{\cos^{-1}(\text{a2p}(x))}{2\pi} = \pm \frac{1}{4}(1 - x) \text{ for } x \in [-1, 1] \quad (14)$$

The phase angles associated to this function are also in the Table 4.

The last step consist in reading the embedded QSP frequencies with a QPE algorithm Fig. 15. A simple trick is used to control the QSP. An alternative solution to control the

⁴It is interesting to note that a2p is the p2a inverse function and vice versa.

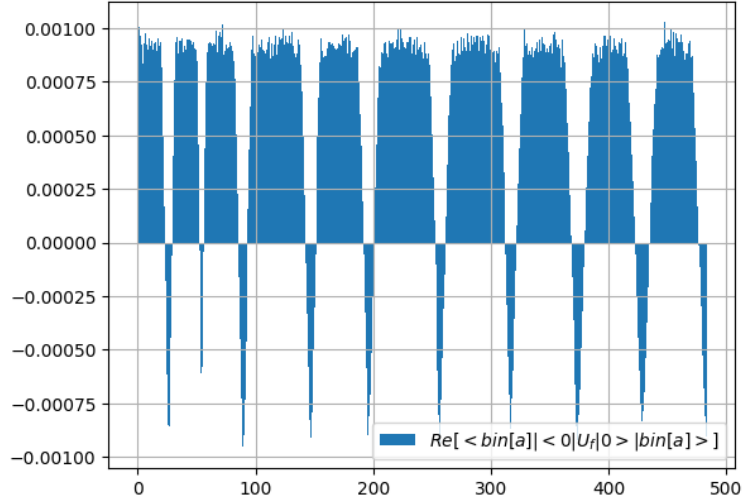
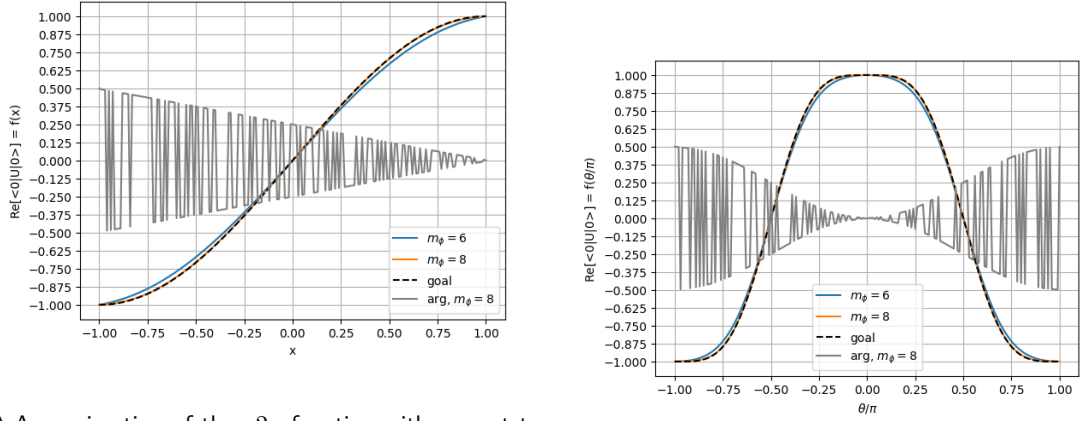


Figure 13: Example of oracle generation to mark the roots of our example function. This diagram was generated with the same strategy as Fig. 10 with the extra embedding of the $\text{step}_{1/10}$ function.



(a) Approximation of the a2p function with respect to the state amplitude function at different degrees m_ϕ .

The phase (grey) resulting from an amplitude image will be proportional to this amplitude.

(b) Approximation of the a2p function with respect to the state eigen-phase function at different degree m_ϕ .

Fig. 15 QSP blocks is to switch from embedded QSP to embedded QSVT [23, Section III]. Embedded QSVT can then simply be controlled by controlling the signal processor gate \widehat{R}_Z and thus divide by two the cost of the circuit.

It is also important to note the numerical error due to the p2a, sgn or a2p function polynomial approximation. It explains the shift of the first wave of Fig. 17. This numerical error is not evaluated in this article. It is nevertheless possible to guess that the error is due mainly due to the arcsin function, which is hard to approximate when $|x| > \frac{1}{2}$ [15, Appendix D]. It can be avoided by choosing different intervals of computing 2.

It is essential to highlight that the binary output will be in a specific format. This format is determined from the value of the two most significant qubits of the \mathcal{F} register. The first indicates the sign of the phase, and the second indicates whether the value is higher or smaller than zero in the amplitude domain, respectively smaller or higher than

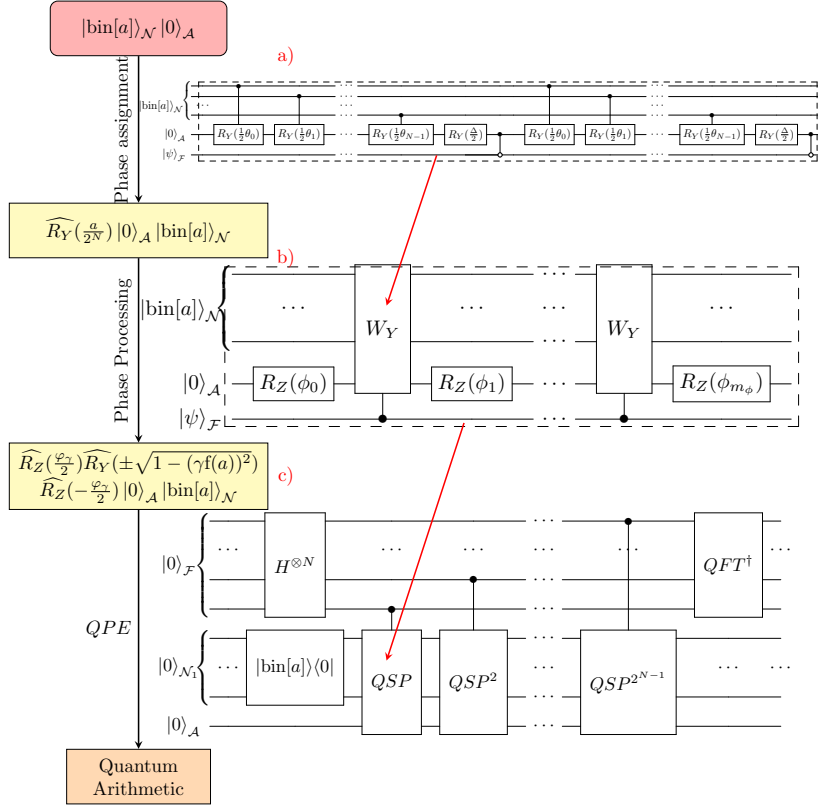


Figure 15: **c)** Full restricted parity QSE quantum circuit. **b)** Controlled-QSP needed for the QSE. **a)** $\widehat{CW_Y}$ controlled signal operator. The control qubit is the one of the \mathcal{F} register. It exploits $\widehat{I} = \widehat{W_Y} \widehat{W_Y}^\dagger$ and $\widehat{W_Y}^\dagger = \widehat{Z} \widehat{W_Y} \widehat{Z}$.

one-fourth. To transform the result in an easy-to-read format⁵, it is required to modify it depending on the area in which the phase is read:

- If the phase lands in the bottom-left area of Fig. 14a: The first two qubits of the \mathcal{F} register read 11b and can be ignored since one-fourth of the easy-to-read format is natively read.
- If the phase lands in the top-left area of Fig. 14a: The first two qubits of the \mathcal{F} register read 01b and a minus sign is implicit since minus one-fourth of the easy-to-read format is natively read.
- If the phase lands in the top-right area of Fig. 14a: The first two qubits of the \mathcal{F} register read 00b, and the value read on the rest of the register is the one complement of the value in the easy-to-read format.
- If the phase lands in the bottom-right area of Fig. 14a: The first two qubits of the \mathcal{F} register read 10b, and the value read on the rest of the register is minus the one complement of the value in the easy-to-read format.

The Fig. 16 indicates how to translate this result in the more straightforward binary representation. The read output is presented in the Fig. 17.

⁵In this work easy-to-read format means positive integer representation plus a bit for the sign.

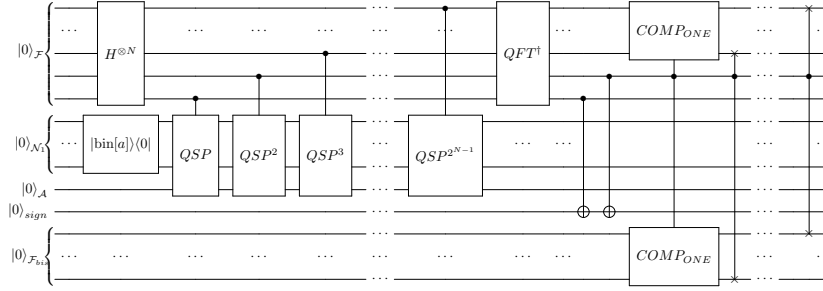


Figure 16: Full restricted parity QSE quantum circuit with the number in an easy-to-read format in the \mathcal{F}_{bis} register. $F_{bis} = F - 1$

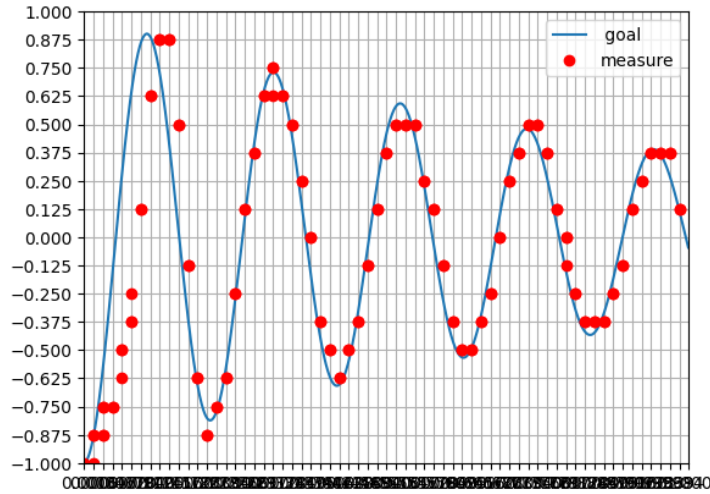


Figure 17: Binary results are read in the \mathcal{F} register and translated in the usual format thanks to Fig. 16. Here $F = 5$ and $N = 6$.

3.2.6 Scaling and Comparison

The results of [15], which construct function polynomial approximations are compared to our results. [15] use binary logic to construct the function approximations. All the [15] registers have the same number of bits ($N = F$) to make the implementation consistent. In their analysis, the figures of merit used are the number of qubits and the count of Toffolly gates, which is representative of the total gate count and of its depth. [15, Appendix B] shows that the Toffolly gate count increases linearly with the polynomial degree p_f if the number of ancilla registers equals the polynomial degree plus one, which means $(p_f + 1)N$ extra qubits. They also explain that a tradeoff between the polynomial degree and the number of ancilla registers exists for a given gate count (and so circuit depth) [15, Table 1] and that seeking this optimal gate count is a complex problem. It is also interesting to mention that the authors propose techniques to accelerate the computing (decreased the circuit depth) thanks to extra qubits and gates.

The scaling of the QSP based technique is detailed in Table 3 under the name of QSE. The table shows that this technique gives better results regarding the qubit number (optimal plus one ancilla) to achieve any polynomial function. It also gives interesting results regarding the number of multiqubit gate scaling with respect to the polynomial

Table 3: Scaling of the QSO and QSE for a fully connected quantum computer. The circuit depth supposes that the two-qubit gate decomposition proposed in the table is used. The QSE depth does not consider the QFT depth, which may vary depending on its implementation.

Operator	Qubit number	Circuit Depth	Gate number				
			\widehat{QFT}_F	\widehat{R}_Z	\widehat{R}_Y	\widehat{CZ}	\widehat{CR}_Y
\widehat{W}_Y	$N + 1$	$N + 1$	0	0	1	0	N
\widehat{QSO}	$N + 1$	$m_\phi(N + 2) + 1$	0	$m_\phi + 1$	m_ϕ	0	$m_\phi N$
\widehat{CW}_Y	$N + 2$	$2(N + 2)$	0	0	2	2	$2N$
\widehat{CQSP}	$N + 2$	$m_\phi(2(N + 2) + 1) + 1$	0	$m_\phi + 1$	$2m_\phi$	$2m_\phi$	$2m_\phi N$
\widehat{QSE}	$F + N + 1$	$2^{F+1}(m_\phi(2(N + 2) + 1) + 1)$	2	$2^{F+1}(m_\phi + 1)$	$2^{F+2}m_\phi$	$2^{F+2}m_\phi$	$2^{F+2}m_\phi N$

degree which is also linear in p_f : $m_\phi = 2p_{p2a} * 2p_{a2p} * 2p_f$. The drawbacks are an overhead due to a2p plus p2a polynomial approximation and a prefactor of the linear scaling (with respect to the polynomial degree) that scales exponentially with the number of digits of the result (F).

3.2.7 Quantum Signal Estimation with Arbitrary Parity

To construct a function without parity constraints, a weighted sum of two QSP (with odd and even function) results can be done (thanks to the LCU technique) in a new qubit register. An arbitrary parity function can also be achieved by choosing an interval two times smaller when going from phase to amplitude so that only one side of the function contains all the function results. This second option is the one used to illustrate the QSE technique in this article Fig. 8, 9b, 13 and 17.

4 Conclusion

This paper presents techniques to construct a Quantum Arithmetic circuit that is not based on binary logic. Although this technique was initially proposed for pedagogical purposes, demonstrating the underlying principles of various quantum computing methods, it results in outcomes that differ significantly from those achieved through binary logic. It could be efficient for specific implementations such as high-order polynomial approximation computed on its input with many digits but with a result expressed with a small number of digits due to the exponential reading overhead. The value on the first digits will not be impacted because the computing aspect and reading of the result are separated.

This work brings a simple geometric interpretation of some quantum computing routines. It explores the equivalence between the different queries to implement quantum information. In particular, it shows how quantum information can be switched from phase to binary domain to be processed and gives a straightforward interpretation of the QFT adder. It also provides a straightforward explanation why a2p and p2a functions appear natively in quantum routines such as QAE or AQE (in HHL) when phase to amplitude transition is needed.

References

- [1] P.W. Shor. “Algorithms for quantum computation: discrete logarithms and factoring”. In Proceedings 35th Annual Symposium on Foundations of Computer Science. Pages 124–134. Santa Fe, NM, USA (1994). IEEE Comput. Soc. Press.

- [2] Lov K. Grover. “A fast quantum mechanical algorithm for database search”. In Proceedings of the twenty-eighth annual ACM symposium on Theory of computing - STOC '96. Pages 212–219. Philadelphia, Pennsylvania, United States (1996). ACM Press.
- [3] Aram W. Harrow, Avinatan Hassidim, and Seth Lloyd. “Quantum algorithm for solving linear systems of equations”. *Physical Review Letters* **103**, 150502 (2009).
- [4] Siyi Wang, Xiufan Li, Wei Jie Bryan Lee, Suman Deb, Eugene Lim, and Anupam Chattopadhyay. “A Comprehensive Study of Quantum Arithmetic Circuits” (2024). arXiv:2406.03867 [quant-ph].
- [5] F. Orts, G. Ortega, E.F. Combarro, and E.M. Garzón. “A review on reversible quantum adders”. *Journal of Network and Computer Applications* **170**, 102810 (2020).
- [6] Vlatko Vedral, Adriano Barenco, and Artur Ekert. “Quantum networks for elementary arithmetic operations”. *Physical Review A* **54**, 147–153 (1996).
- [7] David Beckman, Amalavoyal N. Chari, Srikrishna Devabhaktuni, and John Preskill. “Efficient Networks for Quantum Factoring”. *Physical Review A* **54**, 1034–1063 (1996).
- [8] Thomas G. Draper. “Addition on a Quantum Computer” (2000). arXiv:quant-ph/0008033.
- [9] Lidia Ruiz-Perez and Juan Carlos Garcia-Escartin. “Quantum arithmetic with the Quantum Fourier Transform”. *Quantum Information Processing* **16**, 152 (2017).
- [10] Engin Şahin. “Quantum arithmetic operations based on quantum Fourier transform on signed integers”. *International Journal of Quantum Information* **18**, 2050035 (2020).
- [11] Yewei Yuan, Chao Wang, Bei Wang, Zhao-Yun Chen, Meng-Han Dou, Yu-Chun Wu, and Guo-Ping Guo. “An improved QFT-based quantum comparator and extended modular arithmetic using one ancilla qubit”. *New Journal of Physics* **25**, 103011 (2023).
- [12] Parfait Atchade-Adelomou and Saul Gonzalez. “Efficient Quantum Modular Arithmetics for the ISQ Era” (2023). arXiv:2311.08555 [quant-ph].
- [13] Mehdi Ramezani, Morteza Nikaeen, Farnaz Farman, Seyed Mahmoud Ashrafi, and Alireza Bahrampour. “Quantum multiplication algorithm based on the convolution theorem”. *Physical Review A* **108**, 052405 (2023).
- [14] Philipp Pfeffer. “Comment on “Quantum multiplication algorithm based on the convolution theorem””. *Physical Review A* **110**, 056401 (2024).
- [15] Thomas Häner, Martin Roetteler, and Krysta M. Svore. “Optimizing Quantum Circuits for Arithmetic” (2018). arXiv:1805.12445 [quant-ph].
- [16] Ethan R. Hansen, Sanskriti Joshi, and Hannah Rarick. “Resource Estimation of Quantum Multiplication Algorithms”. In 2023 IEEE International Conference on Quantum Computing and Engineering (QCE). Pages 199–202. (2023).
- [17] Theodore J. Yoder, Guang Hao Low, and Isaac L. Chuang. “Fixed-Point Quantum Search with an Optimal Number of Queries”. *Physical Review Letters* **113**, 210501 (2014).
- [18] Guang Hao Low, Theodore J. Yoder, and Isaac L. Chuang. “Methodology of Resonant Equiangular Composite Quantum Gates”. *Physical Review X* **6**, 041067 (2016).
- [19] Guang Hao Low and Isaac L. Chuang. “Optimal Hamiltonian Simulation by Quantum Signal Processing”. *Physical Review Letters* **118**, 010501 (2017).

- [20] Guang Hao Low and Isaac L. Chuang. “Hamiltonian Simulation by Qubitization”. *Quantum* **3**, 163 (2019).
- [21] John M. Martyn, Zane M. Rossi, Andrew K. Tan, and Isaac L. Chuang. “Grand Unification of Quantum Algorithms”. *PRX Quantum* **2**, 040203 (2021).
- [22] András Gilyén, Yuan Su, Guang Hao Low, and Nathan Wiebe. “Quantum singular value transformation and beyond: exponential improvements for quantum matrix arithmetics”. In *Proceedings of the 51st Annual ACM SIGACT Symposium on Theory of Computing*. Pages 193–204. STOC 2019 New York, NY, USA (2019). Association for Computing Machinery.
- [23] Zane M. Rossi and Isaac L. Chuang. “Semantic embedding for quantum algorithms”. *Journal of Mathematical Physics* **64**, 122202 (2023).
- [24] Sam McArdle, András Gilyén, and Mario Berta. “Quantum state preparation without coherent arithmetic” (2022). [arXiv:2210.14892 \[quant-ph\]](#).
- [25] Richard Cleve, Artur Ekert, Chiara Macchiavello, and Michele Mosca. “Quantum Algorithms Revisited”. *Proceedings of the Royal Society of London. Series A: Mathematical, Physical and Engineering Sciences* **454**, 339–354 (1998).
- [26] Joaquín Ossorio-Castillo, Ulises Pastor-Díaz, and José M. Tornero. “A generalisation of the Phase Kick-Back”. *Quantum Information Processing* **22**, 143 (2023).
- [27] Austin Gilliam, Charlene Venci, Sreraman Muralidharan, Vitaliy Dorum, Eric May, Rajesh Narasimhan, and Constantin Gonceiulea. “Foundational Patterns for Efficient Quantum Computing” (2021). [arXiv:1907.11513 \[quant-ph\]](#).
- [28] Youle Wang, Lei Zhang, Zhan Yu, and Xin Wang. “Quantum Phase Processing and its Applications in Estimating Phase and Entropies”. *Physical Review A* **108**, 062413 (2023).
- [29] Gilles Brassard, Peter Hoyer, Michele Mosca, and Alain Tapp. “Quantum Amplitude Amplification and Estimation”. In Samuel J. Lomonaco and Howard E. Brandt, editors, *Quantum computation and information*. Volume 305, pages 53–74. American Mathematical Society, Providence, RI, 2002. viii+310 pp (2002).
- [30] Rui Chao, Dawei Ding, Andras Gilyen, Cupjin Huang, and Mario Szegedy. “Finding Angles for Quantum Signal Processing with Machine Precision” (2020). [arXiv:2003.02831 \[quant-ph\]](#).
- [31] Yulong Dong, Xiang Meng, K. Birgitta Whaley, and Lin Lin. “Efficient phase-factor evaluation in quantum signal processing”. *Physical Review A* **103**, 042419 (2021).
- [32] Yulong Dong, Lin Lin, Hongkang Ni, and Jiasu Wang. “Robust iterative method for symmetric quantum signal processing in all parameter regimes” (2023). [arXiv:2307.12468 \[quant-ph\]](#).
- [33] Kaoru Mizuta and Keisuke Fujii. “Recursive quantum eigenvalue and singular-value transformation: Analytic construction of matrix sign function by Newton iteration”. *Physical Review Research* **6**, L012007 (2024).
- [34] Shuntaro Yamamoto and Nobuyuki Yoshioka. “Robust Angle Finding for Generalized Quantum Signal Processing” (2024). [arXiv:2402.03016 \[quant-ph\]](#).
- [35] Danial Motlagh and Nathan Wiebe. “Generalized Quantum Signal Processing” (2024). [arXiv:2308.01501 \[quant-ph\]](#).

- [36] N Cody Jones, James D Whitfield, Peter L McMahon, Man-Hong Yung, Rodney Van Meter, Alán Aspuru-Guzik, and Yoshihisa Yamamoto. “Faster quantum chemistry simulation on fault-tolerant quantum computers”. *New Journal of Physics* **14**, 115023 (2012).
- [37] C. H. Bennett. “Logical Reversibility of Computation”. *IBM Journal of Research and Development* **17**, 525–532 (1973).

5 Funding

This research work was supported in part by the French PEPR integrated project Etude de la Pile Quantique — EPIQ, (ANR-22-PETQ-0007).

A Appendix: Phase Angle Series

Efficient ways to search set of phase angles is an active subfield [21, 28, 30–35]. Even if analytical methods exist for a few functions, classical optimization is the straightforward way to seek the phase angles. The set of phase angles proposed in the following appendix was computed using 15 with a parity constraint imposed on the phase angles and thanks to classical optimization. Instead of working in the amplitude domains, it is possible to directly optimize⁶ a function of the phases themselves (16) instead of its associated amplitudes (15):

$$\mathcal{L}(\underline{\phi}) = \sum_{j=0}^d |\text{Re}[\langle 0 | \hat{U}_{\phi}(x_j) | 0 \rangle] - f(x_j)| \text{ with } x_j = \frac{j}{d} \quad (15)$$

$$\mathcal{L}(\underline{\phi}) = \sum_{j=0}^d |\text{Arg}[\langle 0 | \hat{U}_{\phi}(x_j) | 0 \rangle] - f(x_j)| \text{ with } x_j = \frac{j}{d} \quad (16)$$

The main problem of this technique is that little is known on how to constrain the phase angles properties to seek direct phase functions that respect the embedding properties. Other QSP inspired structures, such as QPP [28] or Generalized Quantum Signal Processing (GQSP) [35], could be used; it is nevertheless very likely that it would not allow embedding. The function must thus be computed in one shot.

The following Table 4 gives the article’s function antisymmetric set of phase angles.

⁶It is important to remember that this section deals with classical optimization. This process ‘only’ needs to compute dm_{ϕ} two-by-two matrix product for each function evaluation, which is tractable with a classical computer. $d > m_{\phi}$ and the higher d , the better.

Table 4: Set of phase angles associated with relevant functions. The functions are from amplitude to amplitude.

Function	Degree m_ϕ	Phase Angles
p2a	2 * 3	1.220677134473429 + $\frac{\pi}{2}$, -0.9141986745515728, -1.2955052748350293, 1.2955052748350293, 0.9141986745515728, -1.220677134473429 + $\frac{\pi}{2}$
	2 * 4	0.8681682322909842 + $\frac{\pi}{2}$, 0.4424429404278441, 1.7226820955233317, -0.28367943409333685, 0.28367943409333685, -1.7226820955233317, -0.4424429404278441, -0.8681682322909842 + $\frac{\pi}{2}$
	2 * 8	1.2320580637283647 + $\frac{\pi}{2}$, 0.8252473731446527, -1.1775425298146687, 0.2540914369944401, -1.899907730573736, 0.6454484715597536, -0.4868827734973951, 1.8131545375465181, -1.8131545375465181, 0.4868827734973951, -0.6454484715597536, 1.899907730573736, -0.2540914369944401, 1.1775425298146687, -0.8252473731446527, -1.2320580637283647 + $\frac{\pi}{2}$
a2p	2 * 10	1.3329924058101739 + $\frac{\pi}{2}$, 1.035009436993698, 0.3490884010660929, -0.3586872071383961, -0.5059414117977128, 1.0391369102079064, -1.642759890740595, -1.1252631786120018, 0.33295057920975346, 0.6452181263562808, -0.6452181263562808, -0.33295057920975346, 1.1252631786120018, 1.642759890740595, -1.0391369102079064, 0.5059414117977128, 0.3586872071383961, -0.3490884010660929, -1.035009436993698, -1.3329924058101739 + $\frac{\pi}{2}$
	2 * 3	1.3276443279747514, 1.415148148001756, 1.058648479211631, -1.058648479211631, -1.415148148001756, -1.3276443279747514
	2 * 4	2.318411389939721, -1.328581845947473, -0.8059565062780474, -1.3599512330439159, 1.3599512330439159, 0.8059565062780474, 1.328581845947473, -2.318411389939721
sgn	2 * 4	-0.2640092131936705, 2.18156267897504, 2.245977049120987, -1.811175086662138, 1.811175086662138, -2.245977049120987, -2.18156267897504, 0.2640092131936705
	2 * 8	1.2302357850991548, 1.0336749243518562, 0.11198067732520582, -0.15680734869559498, -0.9578602870885039, 2.0612195475315174, 0.8243803424562862, -0.6554966690623732, 0.6554966690623732, -0.8243803424562862, -2.0612195475315174, 0.9578602870885039, 0.15680734869559498, -0.11198067732520582, -1.0336749243518562, -1.2302357850991548
	2 * 14	0.27882619783038065, 0.36281454618398395, -1.0026301277387055, 0.3541147797152542, 1.6243661292276912, 0.7417194190156123, -1.156030172384029, 1.586825848651674, -0.5126707526970495, 0.26480940875731623, -0.7942611570978513, -0.8276672490175913, 0.3724217902363619, 1.6407210513498245, -1.6407210513498245, -0.3724217902363619, 0.8276672490175913, 0.7942611570978513, -0.26480940875731623, -0.5126707526970495, -1.586825848651674, 1.156030172384029, -0.7417194190156123, -1.6243661292276912, -0.3541147797152542, 1.0026301277387055, -0.36281454618398395, -0.27882619783038065
step _{1/20}	2 * 21	-1.5382973389338346 + $\frac{\pi}{2}$, 2.851477247855508, -0.40984657825729826, -0.5646293285269941, -0.5972560381469758, -0.3918423962119306, 0.055463135947150695, -0.29944961000660675, -2.7921501174003267, -0.03820994975986922, -2.098844136925592, 0.5999852992281652, -0.8290246226574786, 0.018394471278165098, -0.3193690718221374, 2.8179480550390674, 2.656738804493763, -0.26716122886345256, 2.6371127484302086, -0.22243978812718435, -0.07320162044498352, 0.0, 0.07320162044498352, 0.22243978812718435, -2.6371127484302086, 0.26716122886345256, -2.656738804493763, -2.8179480550390674, 0.3193690718221374, -0.018394471278165098, 0.8290246226574786, -0.5999852992281652, 2.098844136925592, 0.03820994975986922, 2.7921501174003267, 0.29944961000660675, -0.055463135947150695, 0.3918423962119306, 0.5972560381469758, 0.5646293285269941, 0.40984657825729826, -2.851477247855508, 1.5382973389338346 + $\frac{\pi}{2}$
step _{1/10}	2 * 17	0.3359251571426454 + $\frac{\pi}{2}$, -0.7053359438019324, -0.2460812016315209, 0.6290659385757417, 0.26513895221650835, 0.9253504197223081, 0.29770494357694177, 0.3113205753649513, -0.08150412617230154, -1.0429304845709697, 0.6119290859635423, 0.2688690150870127, -1.0037188566241908, -0.5852612343222781, 0.2002510054902895, -0.6262504757168341, -1.0305371577280382, 0.0, 1.0305371577280382, 0.6262504757168341, -0.2002510054902895, 0.5852612343222781, 1.0037188566241908, -0.2688690150870127, -0.6119290859635423, 1.0429304845709697, 0.08150412617230154, -0.3113205753649513, -0.29770494357694177, -0.9253504197223081, -0.26513895221650835, -0.6290659385757417, 0.2460812016315209, 0.7053359438019324, -0.3359251571426454 + $\frac{\pi}{2}$
f	2 * 22	-0.7919265959333694, -1.706573438268197, -0.06300361777976618, 0.14616034291649688, -0.945878016693397, -0.9831865238632601, 0.2723337690220768, -0.053752081558436623, -0.6855847965700638, -0.5029559986160452, -0.8898394054092426, 1.2477726224572974, -1.3842149465999596, -0.14604176338531175, -0.4717698081520115, 0.3155662941024413, -0.18845471639572597, -0.2160277263267179, -0.2530703519014686, -0.6397299812266477, -0.4767079419048785, -0.06737297231596824, 0.06737297231596824, 0.4767079419048785, 0.6397299812266477, 0.2530703519014686, 0.2160277263267179, 0.18845471639572597, -0.3155662941024413, 0.4717698081520115, 0.14604176338531175, 1.3842149465999596, -1.2477726224572974, 0.8898394054092426, 0.5029559986160452, 0.6855847965700638, 0.053752081558436623, -0.2723337690220768, 0.9831865238632601, 0.945878016693397, -0.14616034291649688, 0.06300361777976618, 1.706573438268197, 0.7919265959333694

B Annex: Link with other Quantum Routines

As presented in the main paper, the a2p and p2a functions are already known and used in other quantum computing routines. The following section gives more details on these routines.

B.1 Ancilla Quantum Encoding: large angle correction

The AQE, corrected with a p2a done by QSP, used to construct the \widehat{W}_Y signal operator is similar to the one used in the HHL algorithm and in state initialization [24]. It only differs from the AQE presented in Section 2.2 by the techniques used to implement the function and the qubit which controls the Block-Encoding. The correction allows us to get rid of the small angle approximation ($\sin(x) = x$) needed when AQE is used.

Convert superposition of binary numbers in Block-Encoding amplitude encoding is a problem that happens in other quantum routines (such as Quantum Machine Learning (QML) or state initialization). It is interesting to note that it may be cheaper to use the AQE with p2a function based on embedded QSP instead of the AQE based on logical operations for binary to amplitude conversion in other algorithms.

B.2 Link with Quantum Amplitude Estimation

In quantum computing, the Grover operator, later generalized into the QAE operator, allows to construct from arbitrary unitary \widehat{U} , a gate that behaves like qubitized X/Y -rotationnal: $\widehat{W}_{X/Y}$ gates:

$$\widehat{R}_{X/Y}(\theta, \varphi) = \begin{bmatrix} \alpha & -\beta^* \\ \beta & \alpha \end{bmatrix} \begin{matrix} |0\rangle \\ |0_\perp\rangle \end{matrix} \text{ with } \begin{cases} \alpha = \cos(\theta) \\ \beta = \sin(\theta)e^{i\varphi} \end{cases} \quad (17)$$

The initial Grover operator transform, an arbitrary $SU(2)$, the initial state expressed (or projected) in the good state basis:

$$\begin{aligned} \widehat{U} &= \begin{matrix} & |good\rangle & |good_\perp\rangle \\ \begin{bmatrix} \langle good|\psi_i\rangle & \langle good_\perp|\psi_i\rangle \\ \langle good|\psi_{i\perp}\rangle & \langle good_\perp|\psi_{i\perp}\rangle \end{bmatrix} & \begin{matrix} |\psi_i\rangle \\ |\psi_{i\perp}\rangle \end{matrix} \end{matrix} \\ &= \begin{bmatrix} \cos(\gamma)e^{i\varphi_c} & \sin(\gamma)e^{i\varphi_s} \\ -\sin(\gamma)e^{-i\varphi_s} & \cos(\gamma)e^{-i\varphi_c} \end{bmatrix} \begin{matrix} |\psi_i\rangle \\ |\psi_{i\perp}\rangle \end{matrix} \\ &= \widehat{U}_{good}\widehat{U}_{\psi_i}^\dagger \end{aligned} \quad (18)$$

into a qubitized $\widehat{W}_{X/Y}$ signal operator:

$$\begin{aligned} \widehat{G} &= \widehat{S}_{good}\widehat{S}_{\psi_i} \\ &= \begin{bmatrix} -1 & 0 \\ 0 & 1 \end{bmatrix} \begin{bmatrix} 1 - 2|\cos(\gamma)|^2 & 2\sin(\gamma)\cos(\gamma)e^{i\varphi} \\ 2\sin(\gamma)\cos(\gamma)e^{-i\varphi} & 1 - 2|\sin(\gamma)|^2 \end{bmatrix} \\ &= \begin{bmatrix} \cos(2\gamma) & -\sin(2\gamma)e^{i\varphi} \\ \sin(2\gamma)e^{-i\varphi} & \cos(2\gamma) \end{bmatrix} \begin{matrix} |good\rangle \\ |good_\perp\rangle \end{matrix} \\ &= e^{i\frac{\varphi}{2}}(|good\rangle\langle good| - |good_\perp\rangle\langle good_\perp|) e^{i2\gamma(i|good\rangle\langle good_\perp| + h.c.)} \\ &\quad e^{-i\frac{\varphi}{2}}(|good\rangle\langle good| - |good_\perp\rangle\langle good_\perp|) \end{aligned} \quad (19)$$

with $\varphi = \varphi_c - \varphi_s$ and

$$\begin{aligned}\widehat{S}_\psi &= \widehat{U}_\psi \widehat{S}_0 \widehat{U}_\psi^\dagger \\ &= \widehat{I} - 2|\psi\rangle\langle\psi| \\ \widehat{U}_\psi &= |\psi\rangle\langle 0| + |\psi_\perp\rangle\langle 0_\perp|\end{aligned}\tag{20}$$

For such a gate, the phases and amplitudes are always linked thanks to the a2p and p2a functions. QAE algorithm is used to compute the phase 2γ of this gate thanks to QPE from which are extracted the amplitude with the p2a functions [29, Section 4: p.18]⁷. Indeed, the QAE evaluated gate is a specific Grover operator for which instead of knowing $|good\rangle$, \widehat{U} is known⁸:

$$\begin{aligned}|good\rangle &= \widehat{U}|\psi_i\rangle \Leftrightarrow \widehat{U}_{good} = \widehat{U}\widehat{U}_{\psi_i} = \widehat{A} \\ \Rightarrow \langle good|\psi_i\rangle &= \langle\psi_i|\widehat{U}|\psi_i\rangle\end{aligned}\tag{21}$$

If \widehat{U} has already a $\widehat{W}_{X/Y}$ form, it imply:

$$\begin{aligned}\widehat{A}\widehat{S}_0\widehat{A}^\dagger\widehat{S}_{\psi_i} &= \widehat{U}\widehat{S}_{\psi_i}\widehat{U}^\dagger\widehat{S}_{\psi_i} \\ &= \widehat{U}^2\end{aligned}\tag{22}$$

Applying the same oracle transformation with \widehat{U} the result of a QSP in the $\widehat{W}_{X/Y}$ convention leads naturally to a phase anti-symmetrization similarly to the one explained in appendix D.1:

$$\begin{aligned}&\widehat{S}_{0_A}\widehat{U}^\dagger\widehat{S}_{0_A} \\ &= \widehat{S}_{0_A}\widehat{R}_Z(-\phi_0)\prod_{j=1}^{m_\phi}[\widehat{W}_{X/Y}^\dagger\widehat{R}_Z(-\phi_j)]\widehat{S}_{0_A} \\ &= \widehat{S}_{0_A}\widehat{R}_Z(-\phi_0)\widehat{S}_{0_A}\prod_{j=1}^{m_\phi}[\widehat{S}_{0_A}\widehat{W}_{X/Y}^\dagger\widehat{S}_{0_A}\widehat{R}_Z(-\phi_j)\widehat{S}_{0_A}] \\ &= \widehat{R}_Z(-\phi_0)\prod_{j=1}^{m_\phi}[\widehat{W}_{X/Y}\widehat{R}_Z(-\phi_j)]\end{aligned}\tag{23}$$

and so:

$$\begin{aligned}&\widehat{U}\widehat{S}_{0_A}\widehat{U}^\dagger\widehat{S}_{0_A} \\ &= \prod_{j=1}^{m_\phi}[\widehat{R}_Z(\phi_j)\widehat{W}_{X/Y}]\prod_{j=1}^{m_\phi}[\widehat{W}_{X/Y}\widehat{R}_Z(-\phi_j)]\end{aligned}\tag{24}$$

which is an anti-symmetric QSP in the $\widehat{W}_{X/Y}$ convention.

⁷In the original article, the authors seek the square of the amplitude which equal the probability $|\langle good|\psi_i\rangle|^2$ to measure $|good\rangle$ after one application, so they use p2a² function to convert their QPE results.

⁸Interestingly, this techniques can be extended to arbitrary inner product. It is done by taking advantage of: $\widehat{U}_\psi\widehat{U}_\phi^\dagger = |\psi\rangle\langle\phi| + |\psi_\perp\rangle\langle\phi_\perp|$. It leads to:

$$\widehat{U} = \widehat{U}_\psi\widehat{U}_\phi^\dagger\widehat{V} = \begin{bmatrix} \langle\phi|\widehat{V}|\psi\rangle & \langle\phi_\perp|\widehat{V}|\psi\rangle \\ \langle\phi|\widehat{V}|\psi_\perp\rangle & \langle\phi_\perp|\widehat{V}|\psi_\perp\rangle \end{bmatrix} \begin{bmatrix} |\psi\rangle \\ |\psi_\perp\rangle \end{bmatrix}$$

and

$$\widehat{A}\widehat{S}_0\widehat{A}^\dagger\widehat{S}_\psi = \widehat{U}\widehat{S}_\psi\widehat{U}^\dagger\widehat{S}_\psi = \widehat{V}\widehat{S}_\psi\widehat{V}^\dagger\widehat{S}_\phi$$

C Annex Phase Kick-back: Quantum Arithmetic based Hamiltonian Simulation

The Section 2.1 shows how to construct Quantum Arithmetic from the Hamiltonian Simulation of the function. This argument can also be reversed: Quantum Arithmetic is often the most convenient strategy to construct the Hamiltonian Simulation associated with a function. It leads back to the first quantum algorithm proposals which were mainly based on the notion of phase kickback [25] (and [26] for extra algorithm description with this formalism) which general form is detailed in [25, Section 7]. Three phase kickbacks, which behaves like a phase gates, combined with basis change on the control register, also allows the construction of the rotation gate that appears in the Hamiltonian simulation of Hermitian matrices [36, Section 2.1]. Phase kickback is easily explained by developing the Quantum Arithmetic⁹ as a sum of controlled unitary whose phases are proportional to the function images of the control key:

$$\begin{aligned}\widehat{U}_f &= \sum_{x=0}^{2^F} |\text{bin}[x]\rangle \langle \text{bin}[x]| \otimes |\text{bin}[(f(x) + b) \bmod 2^F]\rangle \langle \text{bin}[b]| \\ &= \widehat{C^F} \{ |\text{bin}[x]\rangle \} \otimes \widehat{ADDm_{f(x)}}\end{aligned}\quad (25)$$

This unitary, controlled modular adder is a powerful tool to transform a binary value into the phase of a phase gate. In order to control the kickback factor l , the adder must be applied to the vector of its eigenbasis:

$$\begin{aligned}\{ |\lambda_l\rangle \} &= \left\{ \sum_{x=0}^{2^{q_{nb}}-1} e^{-i \frac{2\pi}{2^{q_{nb}}} l x} |\text{bin}[x]\rangle \right\} \\ &= \{ \widehat{QFT} |\text{bin}[l]\rangle \} \\ &\quad \text{with } l \in \{ 0, 1, 2, \dots, 2^{q_{nb}} \}\end{aligned}\quad (26)$$

so that:

$$\widehat{ADDm_{f(x)}} |\lambda_l\rangle = e^{-i 2\pi l \frac{f(x)}{2^{q_{nb}}}} |\lambda_l\rangle \quad (27)$$

On the computational basis, the eigenvalues of a projection of the gate eigenstate are read. The read eigenphase is thus proportional to the sought phase, and more accurately, the smaller eigenphase ($l = 1$) is equal to the function image. A more straightforward way to understand it is to estimate the phase of this modular adder in a binary fashion:

⁹Note that the operator must leave all the ancilla registers unchanged for a kickback to appear between the superposed state of the control register. The artifact or garbage that can affect the ancilla register can be removed using the following composed Quantum Arithmetic gate:

$$\begin{aligned}\widehat{U}_f & \quad |\text{bin}[x]\rangle |\text{bin}[b]\rangle |0\rangle |0\rangle \\ = \widehat{U}_{cf}^\dagger \widehat{ADDm} \widehat{U}_{cf} & \quad |\text{bin}[x]\rangle |\text{bin}[b]\rangle |0\rangle |0\rangle \\ = \widehat{U}_{cf}^\dagger \widehat{ADDm} & \quad |\text{bin}[x]\rangle |\text{bin}[b]\rangle |\text{bin}[f(x)]\rangle |\beta\rangle \\ = \widehat{U}_{cf}^\dagger & \quad |\text{bin}[x]\rangle |\text{bin}[(f(x) + b) \bmod 2^F]\rangle |\text{bin}[f(x)]\rangle |\beta\rangle \\ = & \quad |\text{bin}[x]\rangle |\text{bin}[(f(x) + b) \bmod 2^F]\rangle |0\rangle |0\rangle\end{aligned}$$

with \widehat{U}_{cf} the circuit directly coming from the classical gates translation into Toffoli gates. This tricks comes from classical reversible computing [37, Table.I].

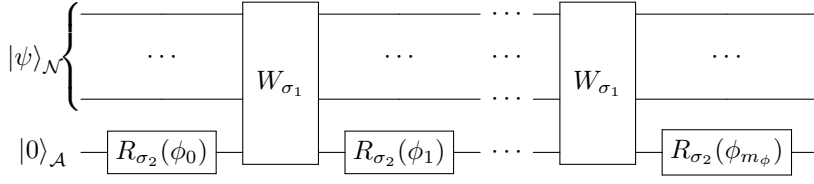


Figure 18: Basic QSP quantum circuit.

$$\begin{aligned}
\hat{I} &= |\text{bin}[(f(x) + b) \bmod 2^F]\rangle \langle \text{bin}[b]|^n \\
&\Leftrightarrow (nf(x) + b) \bmod 2^F = b \\
&\Leftrightarrow \frac{1}{n} = l \frac{f(x)}{2^F}
\end{aligned} \tag{28}$$

These properties are used by Shor's algorithm in which, since multiple of the eigenphase is seeked, a superposition of all the eigenstate except ($l = 0$) can be used:

$$\begin{aligned}
\sum_{l=0}^{2^F-1} \hat{U}_f |\lambda_l\rangle &= |\text{bin}[\alpha]\rangle \\
\text{with } f(\alpha) &= 0
\end{aligned} \tag{29}$$

In Shor's algorithm: $f(x) = e^x \Rightarrow \alpha = 1$

D Annex: Embedded Quantum Signal Processing and Quantum Phase Estimation

D.1 Essential details about Quantum Signal Processing Semantic Embedding

The QSP algorithm allows the processing of the quantum state amplitude real part with a polynomial function [21]. It is done by consecutive repetition of a signal operator \widehat{W}_σ that encodes the problem and a signal processor \widehat{S}_σ with a set of angles depending on the function of interest (30). The polynomial degree is the number of repetitions m_ϕ . The parity of the polynomial is the parity of the number of repetitions. Usually, a Linear Combination of Unitaries (LCU) is done with the odd and even polynomial approximations to achieve an arbitrary polynomial.

$$\begin{aligned}
\widehat{U}_\phi &= \prod_{j=1}^{m_\phi} [\widehat{S}_{\sigma_2}(\phi_j) \widehat{W}_{\sigma_1}] \widehat{S}_{\sigma_2}(\phi_0) \\
&= \widehat{U}_a \begin{bmatrix} P(a) & iQ(a)\sqrt{1-a^2} \\ iQ^*(a)\sqrt{1-a^2} & P^*(a) \end{bmatrix} \widehat{U}_b
\end{aligned} \tag{30}$$

with: $\widehat{U}_a \widehat{\sigma}_1 \widehat{U}_b = \widehat{X}$ and $\widehat{U}_a \widehat{\sigma}_2 \widehat{U}_b = \widehat{Z}$.

P and Q are fixed parity complex polynomials whose order are equal to m_ϕ and $m_\phi - 1$ respectively. The corresponding circuit is illustrated by Fig. 18.

All the angles in the paper come from classical optimization Appendix A.

The primary condition to process amplitudes thanks to QSP is to encode this amplitude thanks to a signal operator qubitized with a Pauli rotation shape (31) and to process it with a signal processor which is perpendicular in the Bloch Sphere. It leads to the QSP

Table 5: The main QSP conventions, the Wx-y convention operator is detailed by (32)

Convention	Signal Operator	Signal processor	Bases change	
	\widehat{W}_{σ_1}	\widehat{S}_{σ_2}	\widehat{U}_a	\widehat{U}_b
Wx	\widehat{W}_X	\widehat{S}_Z	\widehat{I}	
Wy	\widehat{W}_Y	$\widehat{S}\widehat{S}_Z\widehat{S}^\dagger = \widehat{S}_Z$	\widehat{S}	\widehat{S}^\dagger
Wz	\widehat{W}_Z	\widehat{S}_X	\widehat{H}	
Reflection	$\widehat{W}_Y\widehat{Z}$	$\widehat{S}^\dagger\widehat{S}_Z\widehat{S}^\dagger = \widehat{Z}\widehat{S}_Z$	\widehat{S}^\dagger	
Wx-y	$\widehat{W}_{XY\varphi}$	$\widehat{R}_Z(\frac{\varphi}{2})\widehat{S}_Z\widehat{R}_Z(-\frac{\varphi}{2})$	$\widehat{R}_Z(\frac{\varphi}{2})$	$\widehat{R}_Z(-\frac{\varphi}{2})$

conventions of Table 5. It is relevant to remember that other conventions based on different matrices (QSVT [22]) or to different sets of phase angles (GQSP [35] and QPP [28]) exist.

$$\widehat{R}_X(-2\cos^{-1}(a)) = \begin{bmatrix} a & i\sqrt{I-a^2} \\ i\sqrt{I-a^2} & a \end{bmatrix} \begin{matrix} |0\rangle_{\mathcal{A}} \\ |1\rangle_{\mathcal{A}} \end{matrix} \quad (31)$$

$$\widehat{W}_X = \begin{bmatrix} \alpha a & i\sqrt{1-\alpha^2 a^2} \\ i\sqrt{1-\alpha^2 a^2} & \alpha a \end{bmatrix} \begin{matrix} |0\rangle_{\mathcal{A}} |\text{bin}[a]\rangle_{\mathcal{N}} \\ |1\rangle_{\mathcal{A}} |\text{bin}[a]\rangle_{\mathcal{N}} \end{matrix}$$

$$\begin{aligned} \widehat{W}_{XY\varphi} &= \widehat{R}_Z(\varphi)\widehat{W}_X\widehat{R}_Z(-\varphi) \\ &= \begin{bmatrix} A & ie^{i\varphi}\sqrt{I-A^2} \\ ie^{-i\varphi}\sqrt{I-A^2} & A \end{bmatrix} \end{aligned} \quad (32)$$

To process a signal operator with many layers of QSP, the QSP protocol final matrix must keep the shape of a signal operator. A QSP protocol that gives a new signal operator with a known signal processor allows to perform functions of function.

A proposal to construct a semantic embedding of QSP by [23] is to use QSP algorithm with antisymmetric phases angles [23, Section 2, Definition II.3] and starting with a signal operator in the X - Y plan of the Bloch-sphere called twisted oracle [23, Section 2, Definition II.2]. This antisymmetry imposes to process two times more repetitions of the signal operator to achieve the same polynomial degree. It is enough to allows multilayer QSP because:

- $\widehat{W}_{XY\varphi}$ signal operators (32) are a subclass of the operator resulting from a QSP (30): $\widehat{W}_{XY\varphi} \in \widehat{U}_\phi$ with $P = a$ and $Q = e^{i\varphi}$.

- All $\widehat{W}_{XY\varphi}$ signal operators can be processed with the same series of phase angles.

It can be explained because the extra rotations around the Z -axis φ do not cancel each other except for the first and last rotation (30). The first and last rotations do not change the amplitudes of the real part (32).

- The matrix resulting from the antisymmetric QSP of a $\widehat{W}_{XY\varphi}$ signal operator keeps the same shape. As shows by (32) and (34) for one iteration, it is proved by induction starting from the middle of the QSP (35).

Note that this proof also works for even antisymmetric QSP protocol, it begins with a different signal operator: $\widehat{U}_{\phi_0} \leftarrow \widehat{U}_\phi^2$ instead of $\widehat{U}_{\phi_0} \leftarrow \widehat{U}_\phi$.

It is also important to note that P_n remains a real polynom [23, Section 2, Definition II.3].

$$\begin{aligned}\widehat{U}_{\phi\varphi} &= \widehat{R}_Z(\varphi)\widehat{U}_{\phi}\widehat{R}_Z(-\varphi) \\ &= \begin{bmatrix} P(a) & iQ(a)e^{i\varphi}\sqrt{1-a^2} \\ iQ^*(a)e^{-i\varphi}\sqrt{1-a^2} & P(a) \end{bmatrix}\end{aligned}\quad (33)$$

$$\begin{aligned}\widehat{U}_{\phi_2} &= \widehat{U}_{\phi}\widehat{U}_{\phi\varphi}\widehat{U}_{\phi} \\ &= \begin{bmatrix} P_2(a) & iQ_2(a)\sqrt{1-a^2} \\ iQ_2^*(a)\sqrt{1-a^2} & P_2(a) \end{bmatrix} \\ &= \begin{bmatrix} P_2(a) & e^{i\varphi_2}\sqrt{1-P_2(a)^2} \\ e^{-i\varphi_2}\sqrt{1-P_2(a)^2} & P_2(a) \end{bmatrix}\end{aligned}\quad (34)$$

with:

$$\begin{aligned}1 &= P^2 + |Q|^2(1-a^2) \\ P_2 &= P(P^2(2+\cos(\varphi)) - (1+\cos(\varphi))) \\ Q_2 &= Q(2P^2(1+\cos\varphi) - e^{-i\varphi}) \\ e^{i\varphi_2} &= \frac{iQ_2(a)\sqrt{1-a^2}}{\sqrt{1-P_2(a)^2}} \\ \widehat{QSP} &= \dots \widehat{U}_{\phi}\widehat{R}_{Z_2}\widehat{U}_{\phi}\widehat{R}_{Z_1}\widehat{U}_{\phi_0}\widehat{R}_{Z_1}^{\dagger}\widehat{U}_{\phi}\widehat{R}_{Z_2}^{\dagger}\widehat{U}_{\phi}\dots \\ &= \dots \widehat{U}_{\phi}\widehat{R}_{Z_2}\widehat{U}_{\phi}\widehat{U}_{\phi\varphi}\widehat{U}_{\phi}\widehat{R}_{Z_2}^{\dagger}\widehat{U}_{\phi}\dots \\ &= \dots \widehat{U}_{\phi}\widehat{R}_{Z_2}\widehat{U}_{\phi_2}\widehat{R}_{Z_2}^{\dagger}\widehat{U}_{\phi}\dots\end{aligned}\quad (35)$$

Instead of calling QSP inside QSP to produce the embedded QSP, it is equivalently possible to merge the sets of phase angles. It is important to recall that the new set of phase angles is not simply the previous set of phases end-to-end but follows the shape of (36) called phase nesting in [Table 1] [23]. Using:

$$\underline{\phi}_{\gamma}[i, j] = (\phi_{\gamma i}, \phi_{\gamma(i+1)}, \dots, \phi_{\gamma(j-1)}, \phi_{\gamma j})$$

with $j > i$ and $i, j \in [0, m_{\phi_{\gamma}}]$.

$$\begin{aligned}\text{merge}[\underline{\phi}_1, \underline{\phi}_2] &= (\phi_{10} + \phi_{20}, \underline{\phi}_1[1, m_{\phi_1} - 1], \phi_{2,1}, \underline{\phi}_1[1, m_{\phi_1} - 1], \\ &\quad \phi_{22}, \dots, \phi_{2m_{\phi_2-1}}, \underline{\phi}_1[1, m_{\phi_1} - 1], \phi_{1m_{\phi_1}} + \phi_{2m_{\phi_2}})\end{aligned}\quad (36)$$

From this section, when we refer to QSP, it is implicit that the set of phase angles is antisymmetric.

A last but significant remark about antisymmetric QSP is that antisymmetry imposes extra constraints on the functions:

- $P(\pm 1) = 1$ odd antisymmetric QSP.
- $P(0) = \pm 1$ odd antisymmetric QSP.
- $P(\pm 1) = \mp 1$ even antisymmetric QSP.
- $P(0) = 0$ even antisymmetric QSP.

D.2 Important details about Quantum Phase Estimation of a Quantum Signal Processing Semantic Embedding Result

To understand why, for the embedded QSP result, the QPE algorithm can be used to read the state amplitudes, let us remember that the phases read by the QPE $\Phi = \frac{1}{n}$ are defined as each phase that respect (37). Only two phases can be measured in the QSE case: Φ and $-\Phi$. The second phase associated with the other rotational direction is also measured; this phase is $-\frac{1}{n}$, which is measured as the first phase one's complement.

$$\widehat{U}_b \begin{bmatrix} e^{i\Phi_1} & 0 \\ 0 & e^{i\Phi_2} \end{bmatrix} \widehat{U}_b^\dagger = \widehat{U}_\phi^n \text{ with } n_j \text{ so that } 1 = e^{i\Phi_j} \quad (37)$$

Let us also remember that antisymmetric QSP result have a real processed signal and so a basis change: $\widehat{U}_b = \widehat{R}_Z(\varphi)\widehat{H}$. Its phase is linked to its amplitude by the following relation (38).

$$\begin{aligned} \widehat{I} &= \begin{bmatrix} P & \sqrt{1-P^2} \\ \sqrt{1-P^2} & P \end{bmatrix}^n \\ &= \begin{bmatrix} T_n(P) & \sqrt{1-T_n(P)^2} \\ \sqrt{1-T_n(P)^2} & T_n(P) \end{bmatrix} \\ &= \begin{bmatrix} \cos(n \cos^{-1}(P)) & \sqrt{1-T_n(P)^2} \\ \sqrt{1-T_n(P)^2} & \cos(n \cos^{-1}(P)) \end{bmatrix} \\ &\Leftrightarrow 2\pi = \pm n \cos^{-1}(P) \\ &\Leftrightarrow \frac{1}{n} = \pm \frac{\cos^{-1}(P)}{2\pi} \end{aligned} \quad (38)$$